

Surface ozone response to satellite-constrained NO_x emission adjustments and its implications

Changhan Bae¹, Hyun Cheol Kim^{2,3}, Byeong-Uk Kim⁴, and Soontae Kim^{1,*}

¹Department of Environmental and Safety Engineering, Ajou University, Suwon, South Korea

²Air Resources Laboratory, National Oceanic and Atmospheric Administration, College Park, MD, USA

³Cooperative Institute for Climate and Satellites, University of Maryland, College Park, MD, USA

⁴Georgia Environmental Protection Division, Atlanta, GA, USA

Corresponding author: Soontae Kim (soontaekim@ajou.ac.kr)

Abstract. Both surface and satellite observations have shown a decrease in NO_x emissions in East Asian countries in recent years. In order to reflect the recent NO_x emission reduction and to investigate its impact on surface O₃ concentrations in Asian megacities, we adjusted two bottom-up regional emission inventories of which base years are 2006 (E2006) and 2010 (E2010), respectively. We applied direct and relative emission adjustments to both E2006 and E2010 to constrain NO_x emissions using OMI NO₂ vertical column densities. Except for the relative emission adjustment with E2006, modeling results with adjusted emissions exhibit that NO_x emissions over East Asian megacities (Beijing, Shanghai, Seoul, and Tokyo) in the bottom-up inventories are generally overestimated. When the direct emission adjustment is applied to E2006, model biases in the Seoul Metropolitan Area (SMA), South Korea are reduced from 24 ppb to 2 ppb for NO_x (=NO+NO₂) and from -9 ppb to 0 ppb for O₃. In addition, NO₂ model biases in Beijing and Shanghai in China are reduced from 8 ppb and 18 ppb to 0 ppb and 1 ppb, respectively. daily maximum 8-hour average O₃ model biases over the same places are decreased by 8 ppb and 14 ppb. Further analyses suggest that the reduction in domestic South Korean NO_x emissions plays a significant role in increasing O₃ concentrations in SMA. We conclude that the current strong drive to reduce NO_x emissions as part of the strategy to lower particulate matter concentrations in South Korea can account for increased O₃ concentrations in recent years and suggest that more aggressive NO_x emissions will be necessary soon.

Key words.

NO_x emissions; Satellite data; Ozone chemical regime; Control policy

Capsule.

Recent reductions in NO_x emissions over East Asian megacities may have promoted the increase of O₃ concentrations. It implies that insightful emission regulations that consider chemical characteristics are required.

36 **1 Introduction**

37 Surface ozone (O₃) is a critical trace gas found in the troposphere that affects both the biosphere and human health.
38 Tropospheric O₃ can be generated through photochemical reactions of nitrogen oxides (NO_x) and volatile organic
39 compounds (VOCs) in the presence of sunlight. Tropospheric O₃ chemistry is highly nonlinear (Lin et al., 1988;
40 Liu et al., 1987; Sillman et al., 1990). Amounts of photochemically produced O₃ depend on a chemical regime
41 and they are often determined by the ratio of VOCs to NO_x (Sillman, 1999, 1995). O₃ can be removed through the
42 reaction with NO in NO_x-rich environments (i.e., O₃ titration in a NO_x-saturated regime) such as the center of
43 megacities. On the other hand, ozone in a NO_x-sensitive regime (e.g., rural areas) increases with increasing NO_x
44 and responds weakly to an increase in VOC concentrations.

45 In recent years, the amount of anthropogenic NO_x emissions released in East Asia has changed dramatically
46 (Kurokawa et al., 2013; Zhang et al., 2007; Zhao et al., 2013). Following a long-term rise in NO_x emissions from
47 China, a clear reduction has been observed since 2012 (De Foy et al., 2016; Duncan et al., 2016; Krotkov et al.,
48 2016; Miyazaki et al., 2017). The most likely explanation for this is the strong governmental efforts to reduce
49 anthropogenic NO_x emissions, especially in China (Liu et al., 2016). However, few studies have investigated how
50 this rapid change in NO_x emissions has affected regional air quality in the megacities and other areas of East Asia
51 (Li et al., 2019).

52 In the Seoul Metropolitan Area (SMA), the capital region of South Korea, the surface measurements show that
53 daily mean NO and NO₂ concentrations have continuously decreased since 2001 (Supplementary Fig. 1(A)).
54 In contrast, daily maximum 8-hour average (MDA8) O₃ and Ox (=O₃+NO₂) concentrations during ozone seasons
55 have increased. We noted that changes in daily mean NO_x (=NO+NO₂) and MDA8
56 O₃ concentrations show a strong negative correlation. We speculate several reasons that may have led to the O₃
57 increase in SMA: long-range transport, NO_x and VOC emission changes, and meteorology. Among these
58 potential causes of increased ozone concentrations in SMA, we attempt to quantify effects of recent NO_x emission
59 changes by developing regional emission inventories that reflect the most current NO_x condition.

60 Many previous studies have utilized satellite NO₂ column data to estimate and analyze NO_x emissions in East
61 Asia (Beirle et al., 2011; Fioletov et al., 2011; Liu et al., 2016; Liu et al., 2017; Martin et al., 2003; Wang et al.,
62 2012). Top-down emissions data derived from satellite observations can be used to track rapid changes in
63 emissions, but this technique has some limitations. Liu et al. (2017) estimated changes in Chinese NO_x emissions
64 from 2005 to 2015 based on satellite observations, chemical transport model simulations, and bottom-up emissions
65 inventories. They reported that spatial uncertainty in bottom-up emissions inventories affects the quality of top-
66 down emission data. Other studies (e.g., van der A et al. 2008; Liu et al., 2016; Zhang et al. 2007) quantifying
67 NO_x emission trends in China have reported that a number of factors, such as satellite data retrieval algorithms,
68 NO₂ lifetime, and NO/NO₂ ratios can create uncertainties in emission data. Similarly, De Foy et al. (2014)
69 demonstrated that the quality of top-down emission data depends considerably on the methodology and input data
70 employed. Duncan et al. (2013) proposed an alternative approach that uses relative changes in satellite
71 NO₂ column densities over time. However, their methodology still highly depends on the accuracy of bottom-up
72 emission inventories and requires a reliable bottom-up emissions inventory. On the other hand, the methodology
73 is relatively less affected by uncertainty in retrieval algorithms or NO/NO₂ ratios.

74 In this study, we investigated responses of O₃ levels in SMA to recent NO_x emission reductions in East Asia using
75 a three-dimensional chemical transport model (CTM). CTM simulations were used to determine the relationship
76 between NO_x emissions and NO₂ vertical column densities (VCD) when we estimated changes in NO_x emissions
77 (scaling factor; Martin et al., 2003) and responses of surface ozone to these changes. We applied two top-down
78 NO_x emission adjustments: a) direct adjustment using the comparison between the model results and the satellite
79 data, and b) relative adjustment using past and present satellite observations.

80 The rest of this manuscript is structured as follows: the description about model and data in Section 2 including
81 NO_x emission adjustment methods (Section 2.5), the summary of simulation results in Section 3, and the
82 conclusion in Section 4.

83

84 2 Data and Methodology

85 2.1 Overall process

86 In this study, NO_x emissions were adjusted using direct and relative methods based on NO₂ VCD satellite
87 observations and CTM simulations. The Community Multiscale Air Quality (CMAQ) model (Byun and Schere,
88 2006) was used to simulate air pollutant concentrations (see Section 2.2 for details). Tropospheric NO₂ VCD
89 observations from the Ozone Monitoring Instrument (OMI) were used (see Section 2.4 for details). The emission
90 adjustment processes employed for this study are summarized below.

91 (1) Air pollutant simulation was conducted with 2015 meteorological data for the East Asian region using CMAQ
92 based on bottom-up emissions inventories for 2006 and 2010 (see Section 2.3 for details). The simulated NO₂
93 VCDs were calculated using the CMAQ results.

94 (2) The tropospheric NO₂ VCDs observed by the OMI in 2015 were fit to the CMAQ grid. Averaging kernels and
95 conservative downscaling were applied (Kim et al., 2016; see Section 2.4 for details).

96 (3) The ratio between the observed and simulated NO₂ VCDs for each model grid was calculated and used to
97 adjust the bottom-up NO_x emissions (direct adjustment; see Section 2.5 for details). This step produced two
98 emission inventories.

99 (4) The relative changes in satellite NO₂ VCDs from 2006 to 2015 and from 2010 to 2015 were calculated because
100 2006 and 2010 were the baseline years for the emissions inventories. The relative change in NO₂ VCD for each
101 model grid was used to adjust the bottom-up NO_x emissions (relative adjustment; see Section 2.5 for details). This
102 step produced two emission inventories.

103 (5) CMAQ simulations were performed using top-down NO_x emissions derived from (3) and (4).

104 The simulation results with/without the adjusted emissions were evaluated using surface observations in SMA for
105 NO_x and ozone concentrations (see Section 3.2 for details).

106

107 2.2 Chemical transport model

108 To simulate regional air quality in East Asia, we adopted the Weather Research and Forecasting (WRF; Skamarock
109 and Klemp, 2008) and CMAQ modeling system. WRF version 3.4.1 was used for meteorology simulations based
110 on NCEP FNL (Final) Operational Global Analysis data, which was employed for initial and boundary conditions.
111 The WRF model has 35 layers. WRF outputs were converted to CMAQ-ready meteorological inputs with the
112 Meteorology-Chemistry Interface Processor (MCIP; Otte and Pleim, 2010) version 3.6. The WRF vertical layers
113 are mapped to 22 layers in CMAQ. The height of the first layer in CMAQ is 35 m.

114 CMAQ version 4.7.1 was used to simulate chemical reactions and transport. The Sparse Matrix Operator Kernel
115 Emission (SMOKE) was used to process the emission data to prepare hourly gridded emission inputs for CMAQ.
116 The fifth generation CMAQ aerosol module (AERO5) and Statewide Air Pollution Research Center version 99
117 (SAPRC99; Carter, 1999) were used as the aerosol module and the gas-phase chemical mechanism, respectively.
118 The modeling domain covers East Asia with a horizontal resolution of 27 km x 27 km. The boundary conditions
119 for all chemical species were prepared with the CMAQ default profile. Detailed information for the WRF and
120 CMAQ configurations is presented in supplementary Table 1. *Considering the peak ozone season, monsoon
121 season, and the quality of satellite data, we chose to model the period from May 1 to May 31, 2015*

122 2.3 Bottom-up emissions inventories

123 Two emissions inventories were used in the simulations to represent 2006 and 2010 emission levels. For
124 anthropogenic emissions, the Intercontinental Chemical Transport Experiment–Phase B (INTEX-B) 2006
125 emission inventory and the Model Inter-Comparison Study for Asia (MICS-Asia) 2010 emission inventory were
126 used to represent the emissions from Asian countries. Emissions within South Korea in these two Asian inventories
127 were replaced with emission data from the Clean Air Policy Support System’s (CAPSS) emissions inventories for
128 2007 and 2010.

129 The INTEX-B emissions inventory was developed to support the National Aeronautics and Space Administration
130 (NASA) INTEX-B field campaign. Four emissions sectors – power plants, industry, residential, and transportation
131 – are included in the dataset. This inventory covers 22 countries in Asia (<http://mic.greenresource.cn/intex-b2006>)
132 (Zhang et al., 2009). The MICS-Asia emissions inventory was designed to support the MICS-Asia model inter-
133 comparison research. Emission data from 30 countries are incorporated into a mosaic inventory at a uniform
134 spatial and temporal resolution (Li et al., 2017). The CAPSS inventories provide detailed information on South
135 Korean emissions over four emission sectors: point, area, on-road, and non-road. CO, NO_x, SO_x, PM₁₀, and VOC
136 emissions are available (Lee et al., 2011). Total NO_x emissions in CAPSS inventories decreased from 1,187,923
137 tons/year in CAPSS 2007 to 1,061,210 tons/year in CAPSS 2010 over South Korea (11% decrease from 2007)
138 and from 385,398 tons/year in CAPSS 2007 to 291,771 tons/year in CAPSS 2010 over SMA (24% decrease from
139 2007). The Model of Emissions of Gases and Aerosols from Nature (MEGAN; Guenther et al., 2006) was used
140 for biogenic emissions. Fire emissions are not included in the study. However, we examined potential daily fire
141 emission impacts on the emission adjustment using Fire INventory from NCAR (FINN; Wiedinmyer et al., 2011)
142 data and backward trajectory analysis using the HYSPLIT. The results indicate little influences of fire emissions
143 on the simulation results (Supplementary Fig. 2).

144 In summary, the following combinations of emission inventories were employed: INTEX-B 2006 for international
145 sources, CAPSS 2007 for South Korean sources, and MEGAN for biogenic emissions (i.e. E2006); and MICS-
146 Asia 2010 for international sources, CAPSS 2010 for South Korean sources, and MEGAN for biogenic emissions
147 (i.e. E2010).

148 2.4 Satellite observation data

149 To capture realistic recent changes, NO_x emissions were constrained using satellite observations. Tropospheric
150 NO₂ VCD observations from the OMI, which is located onboard the Earth Observing System Aura satellite, were
151 utilized to adjust the bottom-up emissions. The OMI is a nadir-viewing imaging spectrographic instrument used
152 to observe solar backscatter radiation using visible and ultraviolet wavelengths (270–500 nm). We utilized the
153 Dutch OMI NO₂ (DOMINO, version 2.0), retrieved by the Royal Netherlands Meteorological Institute (KNMI)
154 using differential optical absorption spectroscopy (Boersma et al., 2007, 2004). The uncertainty caused by
155 retrieval algorithm is known to be 20–50% (Goldberg et al., 2017; van Noije et al., 2006). Datasets were obtained
156 from the European Space Agency’s Tropospheric Emission Monitoring Internet Service (TEMIS;
157 <http://www.temis.nl/airpollution/no2.html>). Since OMI NO₂ column density products have variable pixel sizes,
158 we applied a conservative spatial regridding method to match with the CMAQ grid cells. The method calculates
159 the fraction of overlapping satellite pixels and model grid cells using a polygon clipping algorithm and performs
160 weighted averaging for each model grid cell (Kim et al., 2016).

161 The appropriate processing of satellite data is vital when comparing results from regional models. For basic data
162 quality control, each satellite pixel was screened using cloud coverage and a data quality flag. Pixels with over
163 40% cloud coverage or contaminated by row anomalies were filtered out.

164 2.5 Emission adjustment methodology

165 Bottom-up emission inventories are constructed using state-of-the-art knowledge of all known emission sources,
166 but no emissions inventory is perfect. In general, bottom-up emissions are estimated with actual observations as
167 well as engineering calculations based on activities, emission factors, and control efficiencies. Therefore, the
168 uncertainty of basic data for engineering calculations could affect the quality of emission inventories. In addition,
169 the pre-processing of emissions inventory for the air quality modeling (e.g. spatial/temporal
170 allocation and/or chemical speciation) can also introduce uncertainties in modeling results.

171 In this respect, we assume two major deficiencies: the incompleteness of the initial dataset and the presence of
172 out-of-date information. To account for these limitations, we designed two emissions adjustment methods. First,
173 we compared satellite NO₂ VCDs with model NO₂ VCDs and then calculated the satellite-to-model ratios for each
174 grid cell. We call this method as the direct adjustment. Two sets of adjustment ratios were generated for the E2006
175 and E2010 emissions inventories. Second, we calculated the relative changes in the satellite NO₂ VCDs between
176 2006 and 2015 and between 2010 and 2015. We call this method as the relative adjustment. The direct and relative
177 adjustment methods were employed using Equations (1) and (2), respectively.

$$E_{\text{NO}_x, \text{direct-adj}} = E_{\text{NO}_x, \text{bottom-up}} \times \left(\frac{\text{NO}_2 \text{VCD}_{\text{obs}, 2015}}{\text{NO}_2 \text{VCD}_{\text{model}, 2015}} \right) \quad (1)$$

179 where, $E_{\text{NO}_x, \text{direct-adj}}$ is the adjusted NO_x emissions based on the direct adjustment method; $E_{\text{NO}_x, \text{bottom-up}}$ is the initial
 180 NO_x emission data used for modeling, which corresponds to E2006 and E210 (moles/grid/month); NO₂
 181 VCD_{obs,2015} is the satellite-based NO₂ VCD observations (molecule/cm²) for 2015; and, NO₂ VCD_{model,2015} is CTM-
 182 based NO₂ VCD simulations (molecule/cm²) for 2015 using the bottom-up emissions inventories.
 183

$$E_{\text{NO}_x, \text{relative-adj}} = E_{\text{NO}_x, \text{bottom-up}} \times \left(\frac{\text{NO}_2 \text{VCD}_{\text{obs}, 2015}}{\text{NO}_2 \text{VCD}_{\text{obs}, \text{EI base year}}} \right) \quad (2)$$

185 Where, $E_{\text{NO}_x, \text{relative-adj}}$ is the adjusted NO_x emissions based on the relative adjustment method and NO₂ VCD_{obs, EI}
 186 _{base year} is the satellite-based NO₂ VCD observations (molecule/cm²) for the base year of each emissions inventory
 187 (2006 or 2010). The definitions of $E_{\text{NO}_x, \text{bottom-up}}$ and NO₂ VCD_{obs,2015} are the same as in Equation (1).
 188

189 We conducted six simulations: two simulations with the original inventory sets and four simulations with the
 190 adjusted NO_x emissions for May 2015:

- 191 (1) Base run using 2006 emissions inventories (E2006)
- 192 (2) Base run using 2010 emissions inventories (E2010)
- 193 (3) Sensitivity run using E2006 with direct NO_x adjustment (E2006-direct_adj)
- 194 (4) Sensitivity run using E2010 with direct NO_x adjustment (E2010-direct_adj)
- 195 (5) Sensitivity run using E2006 with relative NO_x adjustment (E2006-relative_adj; 2006 to 2015)
- 196 (6) Sensitivity run using E2010 with relative NO_x adjustment (E2010-relative_adj; 2010 to 2015).

197 To distinguish impacts of local and foreign emission adjustments on NO₂ and O₃ concentrations over South Korea,
 198 four additional simulations were performed. The impacts have been estimated with differences in NO₂
 199 concentrations simulated from the base run and sensitivity runs as follows.

- 200 (7) Sensitivity run using E2006 with direct NO_x adjustment over South Korea
- 201 (8) Sensitivity run using E2006 with direct domain-wide NO_x adjustment excluding South Korea
- 202 (9) Sensitivity run using E2010 with direct NO_x adjustment over South Korea
- 203 (10) Sensitivity run using E2010 with direct domain-wide NO_x adjustment excluding South Korea.

204
 205 Both adjustment techniques have their advantages and limitations. When the direct adjustment method is applied,
 206 we can construct a more realistic geographical distribution of NO_x emissions. This method, however, is based on
 207 the simple assumption that the change in the NO₂ VCD is the same as the change in NO_x emissions, which is not
 208 always true. As discussed in the previous section, the VCD retrieval algorithm may introduce significant
 209 uncertainties and past studies recognize uncertainties related to the spatial grid resolution and satellite passing
 210 time (Povey and Grainger et al., 2015). Although more complicated approaches based on the NO_x emission-to-
 211 concentration response (e.g., the beta value technique; Lamsal et al., 2011) or local transport have been proposed,
 212 the simple approach used in this study produced obvious improvement of model performance.

213 The relative adjustment technique was used to determine relative changes in NO₂ VCD from the satellite data. In
 214 this approach, we do not need to consider the direct correlation between NO₂ VCD and NO_x emissions because
 215 the beta value (i.e., the correlation between NO₂ VCD and NO_x emissions) would be canceled out in the inter-
 216 annual comparison (Pan et al., 2014). However, it should be noted that meteorological conditions for different
 217 years may affect the retrieval of NO₂ VCDs and its further application. In addition, satellite NO₂ VCD lower than
 218 the detection limit may cause appreciable uncertainty in the emission adjustments due to noise in the satellite data

219 (Steensen et al., 2016). The detection limit of OMI data is reported as $0.5\text{--}1.0 \times 10^{15}$ molecule/cm² (Bucsela et al.,
220 2008). Thus, we excluded those pixels of which NO₂ VCD values are smaller than 1×10^{15} molecule/cm².

221

222 3 Results and discussion

223 3.1 Top-down NO_x emissions

224 In recent years, significant variation in NO_x emissions has been observed in East Asia. Supplementary Fig.
225 1(B) presents clear changes in the spatial distribution of NO₂ VCDs observed by the OMI for 2006, 2010, and
226 2015 in East China and South Korea. Notably, between 2006 and 2010, the NO₂ VCD observations from the OMI
227 show increased levels almost all areas in China whereas the NO₂ VCDs show slightly different changes over
228 different regions in South Korea. The NO₂ VCDs in SMA slightly decreased from 2006 to 2010, while the NO₂
229 VCDs in other regions including Busan in the southeast of South Korea increased slightly. Even within SMA,
230 there are variations with the NO₂ VCD; decreasing in the northern region and increasing at the southern boundary.
231 This may be the combined effect of the overall decrease in NO_x emissions in SMA and the construction of more
232 power plants in Chungnam Province, which is located to the south of SMA. However, because the NO₂ VCD is
233 also sensitive to wind directions and temperatures, more detailed investigation is necessary before any conclusion
234 can be drawn on trends in NO_x emissions in South Korea. From 2010 to 2015, noticeable decreases in the NO₂
235 VCD were observed over China, which is consistent with recent analyses (Duncan et al., 2016; Kim et al., 2015;
236 Krotkov et al., 2016). They argued that this decrease was likely due to emission regulation efforts.

237 Supplementary Fig. 3 presents the spatial distributions of the base NO_x emissions for 2006 and 2010, and changes
238 in NO_x emissions after direct and relative emission adjustments. In general, NO_x emissions decrease in the major
239 megacities in China (e.g., Beijing and Shanghai). It indicates that there are considerable differences in NO_x
240 emissions between the bottom-up emissions and the adjusted emissions based on satellite NO₂ VCDs. Over Seoul
241 and Tokyo, NO_x emission changes are less pronounced than Chinese megacities, except in the E2006_direct_adj
242 case.

243 Fig. 1 compares the NO₂ emissions in major urban areas in East Asia before and after applying the emission
244 adjustment. Emissions for each region is a sum of emissions over all modeling grid cells intersecting each region.
245 SMA NO_x emissions in May 2015, derived from direct adjustment, are 37% lower than in E2006 and 26% higher
246 than in E2010. On the other hand, SMA NO_x emissions in May 2015, derived with the relative adjustment, are
247 reduced by 16% and 15% compared to E2006 and E2010. Beijing and Shanghai NO_x emissions in May 2015,
248 derived with the direct adjustment, are reduced by 32% and 52% compared to E2006 and 41% and 60% compared
249 with E2010, respectively. For Beijing and Shanghai, the relative adjustment also shows changes in emissions in
250 the same direction as the direct adjustment and results in reductions by 33% and 34% compared to E2006, and
251 35% and 53% compared to E2010, respectively. In summary, NO_x emissions by averaging the emissions after
252 adjustments (except for E2006_relative_adj) are: 23 ktons/month for Seoul, 18 ktons/month for Beijing, 23
253 ktons/month in Shanghai, and 8 ktons/month in Tokyo.

254 For the SMA region, NO_x emissions adjusted using the direct method are consistent for both sets of initial
255 emissions inventories. Although the NO_x emissions in E2006 are twice as those in E2010, E2006-direct_adj
256 exhibits a difference of 10% as compared with E2010-direct_adj. On the other hand, the NO_x emissions in E2006-
257 relative_adj are twice as those in E2010-relative_adj for SMA and Tokyo. This is because the uncertainty of the
258 base emission remains after adjustment using the relative adjustment method. Out of the four different adjustment
259 methods, we notice that E2006-relative_adj is an outlier and believe it implies that E2006 might have the lowest
260 fidelity.

261 3.2 Surface NO, NO₂, and O₃ responses

262 Ten CMAQ simulations (two base runs and eight sensitivity runs) were conducted using the NO_x emission
263 adjustment scenarios. The impact of adjusted NO_x emissions on O₃ concentrations in the SMA was captured in
264 the CMAQ simulations. Fig. 2a shows time series of the daily mean and diurnal variations of O₃ concentrations
265 over SMA. The base simulation using the E2006 emissions inventory underestimated the monthly average and
266 daily maximum concentrations, while the simulation using E2010 emissions inventory overestimated the O₃

267 concentrations. The red and blue lines represent the sensitivity simulations using the NO_x emissions adjusted
268 directly and relatively. In both emission scenarios, the direct adjustment method clearly improved the accuracy of
269 the simulated O₃ concentrations. Fig. 2b and 2c present the NO₂ and NO concentrations in SMA over time. In
270 contrast to O₃ concentrations, the NO₂ and NO concentrations were overestimated using the E2006 emissions and
271 underestimated using the E2010 emissions.

272 Table 1 summarizes model performance evaluations on daily mean NO and NO₂ concentrations, and MDA8 O₃
273 concentrations over SMA. With the direct NO_x emission adjustments, model biases for daily mean NO
274 concentrations in SMA are reduced by 10.0 ppb for E2006 (from -11.2 ppb to -1.2 ppb), and 3.0 ppb for 2010
275 (from -4.7 ppb to -1.7 ppb). For daily mean NO₂ concentrations, the model biases are reduced by 9.1 ppb for
276 E2006 (from 11.6 ppb to 2.5 ppb) but increased by 0.9 ppb for E2010 (from -2.1 ppb to 3 ppb). However, it should
277 be noted that the model biases for NO_x concentrations in the SMA are reduced by 21.5 ppb and 5.5 ppb,
278 respectively, with the direct emission adjustments with E2006 and E2010. The same direct NO_x-emission
279 adjustment runs improve model biases for SMA MDA8 O₃ concentrations (from -8.5 ppb to 0.4 ppb for E2006,
280 and from 5.3 ppb to 1.2 ppb for E2010). Other statistics for model performances over SMA are available from Table
281 1. Model performances over South Korea, Beijing, and Shanghai are also provided in Supplementary Table 2. It
282 can be noticed that the direct NO₂ adjustments lead to better model performance than the relative adjustments for
283 SMA.

284 All NO_x emission adjustments result in better NO₂ and O₃ model performance in Beijing and Shanghai
285 (Supplementary Table 2). For example, root mean square errors (RMSEs) for daily mean NO₂ concentrations in
286 Shanghai are 18.3 ppb and 22.5 ppb for the simulations with E2006 and E2010 emissions inventories. When the
287 direct NO_x emission adjustments are applied, the RMSEs become 3.4 ppb and 4.7 ppb, respectively. Model biases
288 for MDA8 O₃ in Shanghai are reduced by 14.3 ppb for E2006 (from -21.9 ppb to -7.6 ppb) and 14.4 ppb for 2010
289 (from -23.8 ppb to -9.4 ppb) with direct NO_x emission adjustments, respectively. Spatial plots present that NO_x
290 emission reductions in East Asian megacities are appreciable, possibly due to overestimation of traffic and
291 residential NO_x emissions in the emissions inventories, and effects of more intensive emission regulations over
292 the populated urban areas (Supplementary Figs. 4, 5, and 6).

293 While being improved with NO_x emission adjustments, model simulations still have difficulties in replicating the
294 observed O₃ concentrations during the evening period (6 p.m. to 10 p.m.), and the same biases happen in the NO
295 and NO₂ concentrations. We suggest two possible reasons that may cause these biases: 1) the diurnal profile of
296 NO_x emissions used to prepare model inputs and/or 2) too early planetary boundary layer (PBL) collapsing in
297 WRF during the evening compared to observations. Previous studies have reported that the simulated PBL heights
298 tend to underestimate the observations during nighttime (Balzarini et al., 2014; Bei et al., 2017).

299 Temporal incommensurability between satellite measurement (i.e. snapshot data) and air quality simulation (24-
300 hour continuous data) for daily variations is often considered the cause of inconsistencies in other
301 studies (Boersma et al., 2009; Povey and Grainger et al., 2015). This issue also affects the calculation of the
302 emission correction factors derived and introduces errors to the ozone simulations in this study. A recent study on
303 nitrogen oxides in South Korea show similar inconsistencies (Goldberg et al., 2019). We note that such
304 discrepancies occur mainly in the evening or early morning and decrease during the daytime when the
305 photochemical reactions become active. However, this issue is beyond the scope of this study and will need to
306 be investigated more thoroughly in future studies.

307 With the NO_x emissions adjustments, O₃ concentrations are increased over SMA. When the NO_x emission
308 adjustments were applied, we re-estimated domain-wide NO_x emissions. Therefore, it is not clear which regional
309 NO_x emission adjustment (either foreign or domestic) results in O₃ increase in SMA. In order to elucidate the
310 effectiveness of regional NO_x emissions adjustments, we added four more CMAQ sensitivity simulations (Runs
311 7~10). When adjusted using the 2015 OMI VCD and CAPSS 2007, NO_x emissions were mostly overestimated
312 (i.e., a negative impact shown in Fig. 3c) except for several regions. This was evident in most major cities,
313 indicating that there have been continuous NO_x reduction efforts in urban locations, especially from mobile
314 sources. The drop of NO_x emissions in cities is likely to have been driven by governmental efforts to reduce these
315 emissions in South Korea (Kim and Lee, 2018). These reduction efforts are highlighted by the changes in the
316 SMA region, where it took more than 10 years to reduce NO_x emissions from mobile sources by replacing diesel
317 buses with compressed natural gas buses. The removal of diesel-fueled garbage collection trucks has also been
318 very effective for reducing NO_x emissions. We also noticed several positive changes (i.e., the underestimation of

319 NO_x emissions) near coastal regions, most of them are located near major point sources including power plants
320 (Dangjin and Samcheok), industrial facilities (Kwangyang), and cement plants (Dangyang and Samcheok). On
321 the other hand, the direct adjustment resulted in increases in NO_x emissions for CAPSS 2010 (Figs. 2b&c and
322 Fig. 3g). We take this as evidence showing that NO_x emissions in the CAPSS 2010 might have been
323 underestimated. With the continuous decline in NO_x emissions as revealed by observations, we suspect that this
324 underestimation is due to the deficiency of the CAPSS 2010 emissions inventories.

325 The response of O₃ had a mostly negative association with changes in surface NO₂ concentration. We hypothesize
326 that most South Korean cities and industrial locations remain NO_x-saturated despite the reduction in NO_x
327 emissions because the decrease in NO_x emissions based on satellite observations resulted in a strong increase in
328 O₃ concentrations in SMA.

329

330 3.3 The chemical regime in the SMA

331 Our hypothesis that SMA is under a NO_x-saturated chemical regime is further supported by observational evidence
332 from the space. Satellite monitoring also suggests that the SMA has a NO_x-saturated chemical regime. Fig. 4
333 shows the distribution of formaldehyde (HCHO) to NO₂ column density ratios retrieved from the OMI. Because
334 HCHO is a product of many VOC oxidation processes, the satellite-observed ratios of the HCHO to NO₂ column
335 density has been used to indicate a chemical regime of an area (Choi et al., 2012; Duncan et al., 2010; Martin et
336 al., 2004). Duncan et al. (2010) classified the chemical regimes of an area as NO_x-saturated for HCHO/NO₂ < 1
337 and as VOC-saturated for HCHO/NO₂ > 2. For the 2015 ozone season, the OMI HCHO/NO₂ ratio was under 1 in
338 the SMA region, indicating that the region was NO_x-saturated. This is consistent with previous studies (Jeon et
339 al., 2014; Jin et al., 2017) and in-situ measurements taken during the MAPS-Seoul field campaign (NIER and
340 NASA, 2017).

341 4 Conclusion

342 In this study, we quantified the effect of NO_x emission adjustment on O₃ concentrations in an East Asian
343 megacities. We utilized two sets of base emissions inventories (E2006 and E2010) that were constrained using
344 NO₂ VCD observations from the OMI satellite. Our findings are summarized as follows:

345

- 346 (1) Using the satellite-constrained NO_x emissions, we improved model performance for surface NO₂ and MDA8
347 O₃ concentrations in the SMA, Beijing, and Shanghai.
- 348 (2) In all the sensitivity tests, surface O₃ responses to increases in NO_x emissions were negative, indicating that
349 these regions are NO_x-saturated. This is consistent with previous studies based on surface and space-borne
350 observations.
- 351 (3) Changes in domestic NO_x emissions have a major impact on the change in O₃ concentrations in South Korean
352 cities.

353 One important implication of these findings is that the current strong governmental drive to reduce NO_x emissions
354 in order to decrease particulate matter levels in South Korea can cause an unexpected increase in O₃ concentrations,
355 especially in the SMA region due to its current chemical regime (i.e. NO_x-saturated). Due to the nonlinearity of
356 the chemical responses in this region, NO_x disbenefit occurs and the beneficial effect of NO_x reduction on
357 particulate matter levels is not guaranteed given that photochemical oxidant may increase nitric acid formation
358 and oxidation of sulfur compounds in the SMA.

359 In conclusion, we emphasize that the increase in O₃ as a response to the reduction in NO_x emissions should not
360 be interpreted as a negative consequence of NO_x reduction efforts. This phenomenon occurs because the SMA has
361 reached a level of high pollution (e.g., it is NO_x-saturated), and so this increase in O₃ is simply a gate to pass
362 during the progress of emission reduction policy implementation. Thus, it is imperative that this consequence
363 should not be used as an argument against emission reduction efforts because the continuous decline in NO_x is
364 essential for the current NO_x-saturated regime to transition to a NO_x-sensitive regime, where a decrease in NO_x
365 emissions will result in a reduction in O₃. To maximize the effectiveness of emission regulations designed to
366 improve air quality in South Korea, the chemical regime needs to be considered with more modeling studies. In
367 this respect, to control O₃, regulation should target both NO_x and VOC emissions. It also emphasizes that frequent
368 updates of the rapidly changing anthropogenic NO_x emissions are required to better understand the changes in
369 surface O₃ concentrations in this region. Methods utilized in this study will be effective for such a modeling study.

370 The results of this study were mainly derived from analyzing ozone responses in SMA. However, NO_x emissions
371 in megacities such as Beijing and Shanghai have decreased similarly to those in SMA (Fig. 1). The chemical
372 regimes in such cities also appear to be NO_x-rich conditions similar to that in the SMA (Fig. 4). Therefore, the
373 results of this study can be useful for establishing emission regulation policies in the megacities of China.

374

375 **Funding**

376 This study was supported by the National Strategic Project-Fine Particle of the National Research Foundation of
377 Korea (NRF) funded by the Ministry of Science and ICT (MSIT), the Ministry of Environment (ME), and the
378 Ministry of Health and Welfare (MOHW) (2017M3D8A1092015).

379

380 **5 References**

- 381 van der A, R.J., Eskes, H.J., Boersma, K.F., van Noije, T.P.C., Van Roozendael, M., De Smedt, I., Peters, D.H.M.U.,
382 Meijer, E.W., 2008. Trends, seasonal variability and dominant NO_x source derived from a ten year record
383 of NO₂ measured from space. *Journal of Geophysical Research*. 113.
384 <https://doi.org/10.1029/2007jd009021>.
- 385 Balzarini, A., Angelini, F., Ferrero, L., Moscatelli, M., Perrone, M. G., Pirovano, G., Riva, G.M., Sangiorgi, G.,
386 Toppetti, A.M., Gobbi, G.P., Bolzacchini, E., 2014. Sensitivity analysis of PBL schemes by comparing
387 WRF model and experimental data. *Geoscientific Model Development Discussions*. 7(5), 6133-6171.
388 <https://doi.org/10.5194/gmdd-7-6133-2014>.
- 389 Bei, N., Wu, J., Elser, M., Tian, F., Cao, J., El-Haddad, I., Li, X., Huang, R., Li, Z., Long, X., Xing, L., Zhao, S.,
390 Tie, X., Prévôt, A.S., Li, G., 2017. Impacts of meteorological uncertainties on the haze formation in
391 Beijing–Tianjin–Hebei (BTH) during wintertime: a case study. *Atmospheric Chemistry and Physics*.
392 17(23), 14579. DOI:10.5194/acp-17-14579-2017
- 393 Beirle, S., Boersma, K.F., Platt, U., Lawrence, M.G., Wagner, T., 2011. Megacity emissions and lifetimes of
394 nitrogen oxides probed from space. *Science*. 333(6050), 1737-1739.
395 <https://doi.org/10.1126/science.1207824>.
- 396 Boersma, K.F., Eskes, H.J., Brinksma, E.J., 2004. Error analysis for tropospheric NO₂ retrieval from
397 space. *Journal of Geophysical Research: Atmospheres*. 109(D4). <https://doi.org/10.1029/2003jd003962>.
- 398 Boersma, K.F., Eskes, H.J., Veefkind, J.P., Brinksma, E.J., Van Der A, R.J., Sneep, M., Van den Oord, G.H.J.,
399 Levelt, P.F., Stammes, P., Gleason, J.F., Bucsela, E.J., 2007. Near-real time retrieval of tropospheric NO₂
400 from OMI. *Atmospheric Chemistry and Physics*. 7(8), 2103-2118. [https://doi.org/10.5194/acpd-6-12301-](https://doi.org/10.5194/acpd-6-12301-2006)
401 [2006](https://doi.org/10.5194/acpd-6-12301-2006).
- 402 Boersma, K. F., Jacob, D. J., Trainic, M., Rudich, Y., DeSmedt, I., Dirksen, R., Eskes, H. J., 2009. Validation of
403 urban NO₂ concentrations and their diurnal and seasonal variations observed from the SCIAMACHY and
404 OMI sensors using in situ surface measurements in Israeli cities. *Atmospheric Chemistry and*
405 *Physics*. 9(12), 3867-3879. <https://doi.org/10.5194/acp-9-3867-2009>.
- 406 Bucsela, E.J., Perring, A.E., Cohen, R.C., Boersma, K.F., Celarier, E.A., Gleason, J.F., Wenig, M.O., Bertram, T.
407 H., Wooldridge, P.J., Dirksen, R., Veefkind, J.P., 2008. Comparison of tropospheric NO₂ from in situ
408 aircraft measurements with near-real-time and standard product data from OMI. *Journal of Geophysical*
409 *Research: Atmospheres*. 113(D16). <https://doi.org/10.1029/2007JD008838>.
- 410 Byun, D., Schere, K.L., 2006. Review of the Governing Equations, Computational Algorithms, and Other
411 Components of the Models-3 Community Multiscale Air Quality (CMAQ) Modeling System. *Applied*
412 *mechanics reviews*. 59(2), 51-77. <https://doi.org/10.1115/1.2128636>.
- 413 Carter, W.P.L., 1999. Documentation of the SAPRC-99 Chemical Mechanism for VOC Reactivity Assessment.
414 Report to California Air Resources Board. Contracts 92-329 and 95-308.
- 415 Chen, F., Dudhia, J., 2001. Coupling an advanced land surface-hydrology model with the Penn State-NCAR MM5
416 modeling system. Part I: Model implementation and sensitivity. *Monthly Weather Review*. 129(4), 569-
417 585. [https://doi.org/10.1175/1520-0493\(2001\)129<0587:caalsh>2.0.co;2](https://doi.org/10.1175/1520-0493(2001)129<0587:caalsh>2.0.co;2).
- 418 Choi, Y., Kim, H., Tong, D., Lee, P., 2012. Summertime weekly cycles of observed and modeled NO_x and O₃
419 concentrations as a function of satellite-derived ozone production sensitivity and land use types over the
420 Continental United States. *Atmospheric Chemistry and Physics*. 12(14), 6291-6307.
421 <https://doi.org/10.5194/acp-12-6291-2012>.
- 422 Chou, M.D., Suarez, M.J., 1994. An efficient thermal infrared radiation parameterization for use in general
423 circulation models. 1-85.

- 424 De Foy, B., Wilkins, J.L., Lu, Z., Streets, D.G., Duncan, B.N., 2014. Model evaluation of methods for estimating
425 surface emissions and chemical lifetimes from satellite data. *Atmospheric Environment*. 98, 66-77.
426 <https://doi.org/10.1016/j.atmosenv.2014.08.051>.
- 427 De Foy, B., Lu, Z., Streets, D.G., 2016. Satellite NO₂ retrievals suggest China has exceeded its NO_x reduction
428 goals from the twelfth Five-Year Plan. *Scientific reports*. 6, 35912. <https://doi.org/10.1038/srep35912>.
- 429 Duncan, B.N., Yoshida, Y., Olson, J.R., Sillman, S., Martin, R.V., Lamsal, L., Hu, Y., Pickering, K.E., Retscher,
430 C., Allen, D.J., Crawford, J.H., 2010. Application of OMI observations to a space-based indicator of NO_x
431 and VOC controls on surface ozone formation. *Atmospheric Environment*. 44, 2213–2223.
432 <https://doi.org/10.1016/j.atmosenv.2010.03.010>.
- 433 Duncan, B.N., Yoshida, Y., de Foy, B., Lamsal, L.N., Streets, D.G., Lu, Z., Pickering, K.E., Krotkov, N.A., 2013.
434 The observed response of Ozone Monitoring Instrument (OMI) NO₂ columns to NO_x emission controls
435 on power plants in the United States: 2005–2011. *Atmospheric Environment*. 81, 102-111.
436 <https://doi.org/10.1016/j.atmosenv.2013.08.068>.
- 437 Duncan, B.N., Lamsal, L.N., Thompson, A.M., Yoshida, Y., Lu, Z., Streets, D.G., Hurwitz, M.M., Pickering, K.E.,
438 2016. A space-based, high-resolution view of notable changes in urban NO_x pollution around the world
439 (2005-2014): Notable changes in urban NO_x pollution. *Journal of Geophysical Research: Atmospheres*.
440 121, 976–996. <https://doi.org/10.1002/2015jd024121>.
- 441 Fioletov, V.E., McLinden, C.A., Krotkov, N., Moran, M.D., Yang, K., 2011. Estimation of SO₂ emissions using
442 OMI retrievals. *Geophysical Research Letters*. 38(21). <https://doi.org/10.1029/2011gl049402>.
- 443 Goldberg, D.L., Lamsal, L.N., Loughner, C.P., Swartz, W.H., Lu, Z., Streets, D.G., 2017. A high-resolution and
444 observationally constrained OMI NO₂ satellite retrieval. *Atmospheric Chemistry and Physics*. 17(18),
445 11403-11421. <https://doi.org/10.5194/acp-17-11403-2017>.
- 446 Guenther, A., Karl, T., Harley, P., Wiedinmyer, C., Palmer, P.I., Geron, C., 2006. Estimates of global terrestrial
447 isoprene emissions using MEGAN (Model of Emissions of Gases and Aerosols from
448 Nature). *Atmospheric Chemistry and Physics*. 6(11), 3181-3210. [https://doi.org/10.5194/acpd-6-107-](https://doi.org/10.5194/acpd-6-107-2006)
449 2006.
- 450 Hong, S.Y., Dudhia, J., Chen, S.H., 2004. A revised approach to ice microphysical processes for the bulk
451 parameterization of clouds and precipitation. *Monthly Weather Review*. 132(1), 103-120.
452 [https://doi.org/10.1175/1520-0493\(2004\)132<0103:aratim>2.0.co;2](https://doi.org/10.1175/1520-0493(2004)132<0103:aratim>2.0.co;2).
- 453 Hong, S.Y., Noh, Y., Dudhia, J., 2006. A new vertical diffusion package with an explicit treatment of entrainment
454 processes. *Monthly weather review*. 134(9), 2318-2341. <https://doi.org/10.1175/mwr3199.1>.
- 455 Jeon, W.B., Lee, S.H., Lee, H., Park, C., Kim, D. H., Park, S.Y., 2014. A study on high ozone formation mechanism
456 associated with change of NO_x/VOCs ratio at a rural area in the Korean Peninsula. *Atmospheric*
457 *Environment*. 89, 10-21. <https://doi.org/10.1016/j.atmosenv.2014.02.005>.
- 458 Jin, X., Fiore, A.M., Murray, L.T., Valin, L.C., Lamsal, L.N., Duncan, B., Folkert Boersma, K., De Smedt, I., Abad,
459 G.G., Chance, K., Tonnesen, G.S., 2017. Evaluating a space-Based Indicator of surface Ozone-NO_x-VOC
460 sensitivity over midlatitude source regions and application to decadal trends: Space-based indicator of O₃
461 sensitivity. *Journal of Geophysical Research: Atmospheres*. 122(19), 10439-10461.
462 <https://doi.org/10.1002/2017jd026720>.
- 463 Kim, H.C., Lee, P., Kim, S., Mok, J., Yoo, H.L., Bae, C., Kim, B.U., Lim, Y.K., Woo, J.H., Park, R., 2015.
464 Satellite-observed NO₂, SO₂, and HCHO vertical column densities in East Asia: recent changes and
465 comparisons with regional model. American Geophysical Union, Fall Meeting.
- 466 Kim, H.C., Lee, P., Judd, L., Pan, L., Lefer, B., 2016. OMI NO₂ column densities over North American urban
467 cities: the effect of satellite footprint resolution. *Geoscientific Model Development*. 9, 1111–1123.

- 468 <https://doi.org/10.5194/gmd-9-1111-2016>.
- 469 Kim, Y. P., Lee, G., 2018. Trend of air quality in Seoul: Policy and science. *Aerosol Air Qual. Res.* 18, 2141-2156.
470 <https://doi.org/10.4209/aaqr.2018.03.0081>.
- 471 Krotkov, N.A., McLinden, C.A., Li, C., Lamsal, L.N., Celarier, E.A., Marchenko, S.V., Swartz, W.H., Bucsela,
472 E.J., Joiner, J., Duncan, B.N., Boersma, K.F., Veefkind, J.P., Levelt, P.F., Fioletov, V.E., Dickerson, R.R.,
473 He, H., Lu, Z., Streets, D.G., 2016. Aura OMI observations of regional SO₂ and NO₂ pollution changes
474 from 2005 to 2015. *Atmospheric Chemistry and Physics*. 16, 4605–4629. [https://doi.org/10.5194/acp-16-](https://doi.org/10.5194/acp-16-4605-2016)
475 [4605-2016](https://doi.org/10.5194/acp-16-4605-2016).
- 476 Kurokawa, J., Ohara, T., Morikawa, T., Hanayama, S., Janssens-Maenhout, G., Fukui, T., Kawashima, K.,
477 Akimoto, H., 2013. Emissions of air pollutants and greenhouse gases over Asian regions during 2000–
478 2008: Regional Emission inventory in ASia (REAS) version 2. *Atmospheric Chemistry and Physics*. 13,
479 11019–11058. <https://doi.org/10.5194/acp-13-11019-2013>.
- 480 Lamsal, L.N., Martin, R.V., Padmanabhan, A., van Donkelaar, A., Zhang, Q., Sioris, C.E., Chance, K., Kurosu,
481 T.P., Newchurch, M.J., 2011. Application of satellite observations for timely updates to global
482 anthropogenic NO_x emission inventories. *Geophysical Research Letters*. 38(5).
483 <https://doi.org/10.1029/2010gl046476>.
- 484 Lee, D.G., Lee, Y.M., Jang, K.W., Yoo, C., Kang, K.H., Lee, J.H., Jung, S.W., Park, J.M., Lee, S.B., Han, J.S.,
485 Hong, J.H., Lee, S.J., 2011. Korean national emissions inventory system and 2007 air pollutant emissions.
486 *Asian Journal of Atmospheric Environment*. 5, 278–291. <https://doi.org/10.5572/ajae.2011.5.4.278>.
- 487 Li, M., Zhang, Q., Kurokawa, J., Woo, J.H., He, K., Lu, Z., Ohara, T., Song, Y., Streets, D.G., Carmichael, G.R.,
488 Cheng, Y., Hong, C., Huo, H., Jiang, X., Kang, S., Liu, F., Su, H., Zheng, B., 2017. MIX: a mosaic Asian
489 anthropogenic emission inventory under the international collaboration framework of the MICS-Asia and
490 HTAP. *Atmospheric Chemistry and Physics*. 17, 935–963. <https://doi.org/10.5194/acp-17-935-2017>.
- 491 Li, K., Jacob, D.J., Liao, H., Shen, L., Zhang, Q., Bates, K.H., 2019. Anthropogenic drivers of 2013–2017 trends
492 in summer surface ozone in China. *Proceedings of the National Academy of Sciences*. 116(2), 422-427.
493 <https://doi.org/10.1073/pnas.1812168116>.
- 494 Lin, X., Trainer, M., Liu, S.C., 1988. On the nonlinearity of the tropospheric ozone production. *Journal of*
495 *Geophysical Research: Atmospheres*. 93(D12), 15879-15888.
496 <https://doi.org/10.1029/jd093id12p15879>.
- 497 Liu, F., Zhang, Q., Zheng, B., Tong, D., Yan, L., Zheng, Y., He, K., 2016. Recent reduction in NO_x emissions over
498 China: synthesis of satellite observations and emission inventories. *Environmental Research*
499 *Letters*. 11(11), 114002. <https://doi.org/10.1088/1748-9326/11/11/114002>.
- 500 Liu, F., Beirle, S., Zhang, Q., Zheng, B., Tong, D., He, K., 2017. NO_x emission trends over Chinese cities
501 estimated from OMI observations during 2005 to 2015. *Atmospheric chemistry and physics*. 17(15),
502 9261-9275. <https://doi.org/10.5194/acp-2017-369>.
- 503 Liu, S.C., Trainer, M., Fehsenfeld, F.C., Parrish, D.D., Williams, E.J., Fahey, D.W., Hybler, G., Murphy, P.C.,
504 1987. Ozone production in the rural troposphere and the implications for regional and global ozone
505 distributions. *Journal of Geophysical Research: Atmospheres*. 92(D4), 4191-4207.
506 <https://doi.org/10.1029/jd092id04p04191>.
- 507 Martin, R.V., Jacob, D.J., Chance, K., Kurosu, T.P., Palmer, P.I., Evans, M.J., 2003. Global inventory of nitrogen
508 oxide emissions constrained by space-based observations of NO₂ columns. *Journal of Geophysical*
509 *Research: Atmospheres*. 108(D17). <https://doi.org/10.1029/2003jd003453>.
- 510 Martin, R.V., 2004. Evaluation of GOME satellite measurements of tropospheric NO₂ and HCHO using regional
511 data from aircraft campaigns in the southeastern United States. *Journal of Geophysical Research*. 109.

- 512 <https://doi.org/10.1029/2004jd004869>.
- 513 Miyazaki, K., Eskes, H., Sudo, K., Boersma, K.F., Bowman, K., Kanaya, Y., 2017. Decadal changes in global
514 surface NO_x emissions from multi-constituent satellite data assimilation. *Atmospheric chemistry and*
515 *physics*. 17(2), 807-837. <https://doi.org/10.5194/acp-2016-529>.
- 516 National Institute of Environmental Research and the National Aeronautics and Space Administration, 2017.
517 KORUS-AQ Rapid Science Synthesis Report (English). 9-13.
- 518 National Centers for Environmental Prediction, 2000. NCEP FNL Operational Model Global Tropospheric Analyses,
519 continuing from July 1999, Research Data Archive at the National Center for Atmospheric Research,
520 Computational and Information Systems Laboratory. <https://doi.org/10.5065/D6M043C6>.
- 521 van Noije, T.P.C., Eskes, H.J., Dentener, F.J., Stevenson, D.S., Ellingsen, K., Schultz, M.G., Wild, O., Amann, M.,
522 Atherton, C.S., Bergmann, D.J., Bey, I., Boersma, K.F., Butler, T., Cofala, J., Drevet, J., Fiore, A.M.,
523 Gauss, M., Hauglustaine, D.A., Horowitz, L.W., Isaksen, I.S.A., Krol, M.C., Lamarque, J.-F., Lawrence,
524 M.G., Martin, R.V., Montanaro, V., Müller, J.-F., Pitari, G., Prather, M.J., Pyle, J.A., Richter, A., Rodriguez,
525 J.M., Savage, N.H., Strahan, S.E., Sudo, K., Szopa, S., van Roozendaal, M., 2006. Multi-model ensemble
526 simulations of tropospheric NO₂ compared with GOME retrievals for the year 2000. *Atmospheric*
527 *Chemistry and Physics*. 6, 2943–2979. <https://doi.org/10.5194/acpd-6-2965-2006>.
- 528 Otte, T.L., Pleim, J.E., 2010. The Meteorology-Chemistry Interface Processor (MCIP) for the CMAQ modeling
529 system: updates through MCIPv3.4.1. *Geoscientific Model Development*. 3(1), 243-256.
530 <https://doi.org/10.5194/gmd-3-243-2010>.
- 531 Pan, L., Tong, D., Lee, P., Kim, H.C., Chai, T., 2014. Assessment of NO_x and O₃ forecasting performances in the
532 US National Air Quality Forecasting Capability before and after the 2012 major emissions
533 updates. *Atmospheric environment*. 95, 610-619. <https://doi.org/10.1016/j.atmosenv.2014.06.020>.
- 534 Povey, A.C., and Grainger, R.G., 2015. Known and unknown unknowns: uncertainty estimation in satellite remote
535 sensing. *Atmospheric Measurement Techniques*. 8(11). <https://doi.org/10.5194/amt-8-4699-2015>.
- 536 Seinfeld, J.H., 1989. Urban air pollution: State of the science. *Science*. 243, 745–752.
537 <https://doi.org/10.1126/science.243.4892.745>.
- 538 Sillman, S., Logan, J.A., Wofsy, S.C., 1990. The sensitivity of ozone to nitrogen oxides and hydrocarbons in
539 regional ozone episodes. *Journal of Geophysical Research: Atmospheres*. 95(D2), 1837-1851.
540 <https://doi.org/10.1029/jd095id02p01837>.
- 541 Sillman, S., 1995. The use of NO_y, H₂O₂, and HNO₃ as indicators for ozone-NO_x-hydrocarbon sensitivity in urban
542 locations. *Journal of Geophysical Research: Atmospheres*. 100(D7), 14175-14188.
543 <https://doi.org/10.1029/94jd02953>.
- 544 Sillman, S., 1999. The relation between ozone, NO_x and hydrocarbons in urban and polluted rural
545 environments. *Atmospheric Environment*. 33(12), 1821-1845. [https://doi.org/10.1016/s1352-](https://doi.org/10.1016/s1352-2310(98)00345-8)
546 [2310\(98\)00345-8](https://doi.org/10.1016/s1352-2310(98)00345-8).
- 547 Skamarock, W.C., Klemp, J.B., 2008. A time-split nonhydrostatic atmospheric model for weather research and
548 forecasting applications. *Journal of computational physics*. 227(7), 3465-3485.
549 <https://doi.org/10.1016/j.jcp.2007.01.037>.
- 550 Steensen, B. M., Schulz, M., Theys, N., Fagerli, H., 2016. A model study of the pollution effects of the first 3
551 months of the Holuhraun volcanic fissure: comparison with observations and air pollution
552 effects. *Atmospheric Chemistry and Physics*. 16(15), 9745-9760. [https://doi.org/10.5194/acp-16-9745-](https://doi.org/10.5194/acp-16-9745-2016)
553 [2016](https://doi.org/10.5194/acp-16-9745-2016).
- 554 Wang, S.W., Zhang, Q., Streets, D.G., He, K.B., Martin, R.V., Lamsal, L.N., Chen, D., Lei, Y., Lu, Z., 2012.

555 Growth in NO_x emissions from power plants in China: bottom-up estimates and satellite observations.
556 Atmospheric Chemistry and Physics. 12, 4429–4447. <https://doi.org/10.5194/acp-12-4429-2012>.

557 Wiedinmyer, C., S.K. Akagi, R.J. Yokelson, L.K. Emmons, J.A. Al-Saadi, Orlando, J.J. Soja, A.J., 2011. The Fire
558 INventory from NCAR (FINN): a high resolution global model to estimate the emissions from open
559 burning. Geoscientific Model Development. 4, 625-641. <https://doi.org/10.5194/gmd-4-625-2011>.

560 Zhang, Q., Streets, D.G., He, K., Wang, Y., Richter, A., Burrows, J.P., Uno, I., Jang, C.J., Chen, D., Yao, Z., Lei,
561 Y., 2007. NO_x emission trends for China, 1995–2004: The view from the ground and the view from space.
562 Journal of Geophysical Research. 112. <https://doi.org/10.1029/2007jd008684>.

563 Zhang, Q., Streets, D.G., Carmichael, G.R., He, K.B., Huo, H., Kannari, A., Klimont, Z., Park, I.S., Reddy, S., Fu,
564 J.S., Chen, D., Duan, L., Lei, Y., Wang, L.T., Yao, Z.L., 2009. Asian emissions in 2006 for the NASA
565 INTEX-B mission. Atmospheric Chemistry and Physics. 23. <https://doi.org/10.5194/acp-9-5131-2009>.

566 Zhao, B., Wang, S.X., Liu, H., Xu, J.Y., Fu, K., Klimont, Z., Hao, J.M., He, K.B., Cofala, J., Amann, M., 2013.
567 NO_x emissions in China: historical trends and future perspectives. Atmospheric Chemistry and Physics.
568 13, 9869–9897. <https://doi.org/10.5194/acp-13-9869-2013>.

569

570

571 **Table 1.**

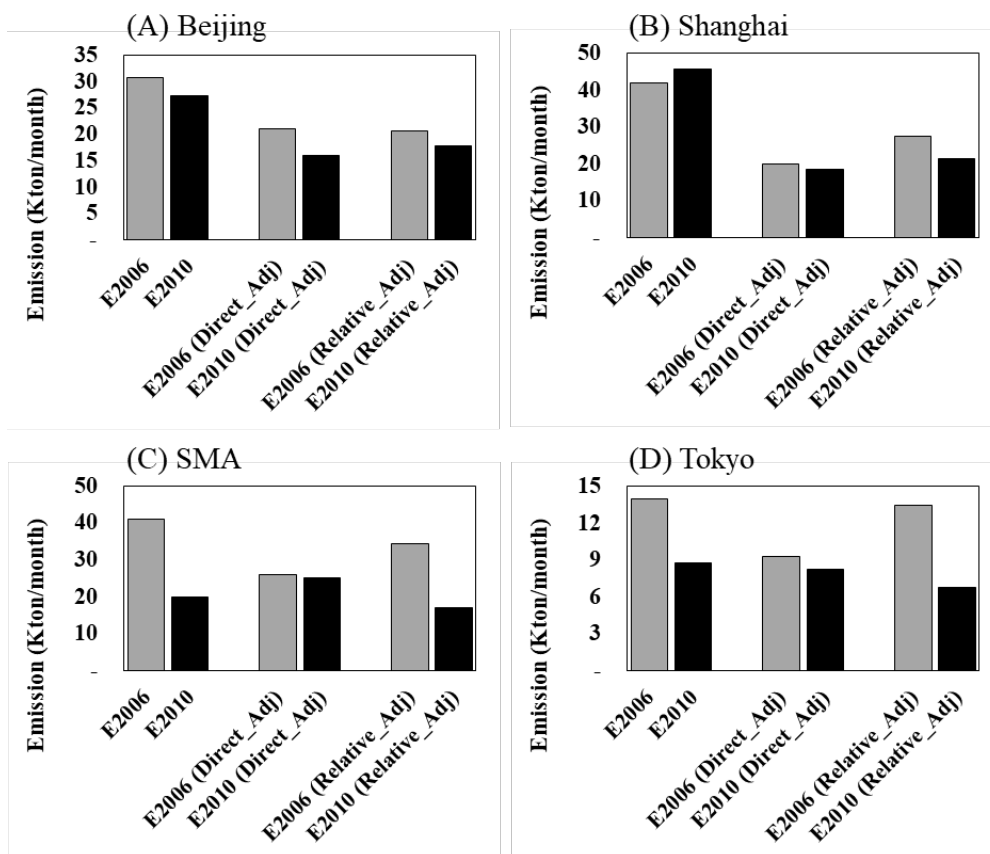
572 Model performance statistics for daily mean NO, daily mean NO₂, and MDA8 O₃ in the SMA in May 2015. The
 573 monthly mean observed concentrations are shown in parentheses. Base CMAQ simulations use both the E2006
 574 (INTEX-B 2006/CAPSS 2007) and E2010 (MICS-Asia 2010/CAPSS 2010) emissions inventories. Direct_adj and
 575 Relative_adj denote NO_x emissions adjustments based on the direct and relative adjustment methods, respectively.
 576 Bold characters indicate the model with the best statistics.

		Base		Direct adjust		Relative adjust	
		E2006	E2010	E2006	E2010	E2006	E2010
Daily mean NO (Observation: 8.6 ppb)	BIAS	11.2	-4.7	-1.2	-1.7	5.1	-5.6
	RMSE	13.4	5.8	3.5	3.5	7.0	6.6
	NME	133.7	55.1	30.7	32.6	68.1	64.7
	R	0.63	0.71	0.66	0.70	0.65	0.74
Daily mean NO ₂ (Observation: 28.2 ppb)	BIAS	11.6	-2.1	2.5	3.0	6.6	-5.2
	RMSE	13.1	5.5	5.8	6.2	8.6	7.0
	NME	42.2	16.0	15.7	16.8	25.6	20.8
	R	0.78	0.75	0.77	0.76	0.79	0.76
MDA8 O ₃ (Observation: 55.6 ppb)	BIAS	-8.5	5.3	0.4	1.2	-4.5	6.7
	RMSE	14.1	11.2	9.9	9.8	11.3	10.9
	NME	20.0	17.0	14.7	14.6	15.7	16.5
	R	0.25	0.48	0.43	0.45	0.35	0.59

Unit = BIAS, RMSE: ppb, Normalized Mean Error (NME): %, R

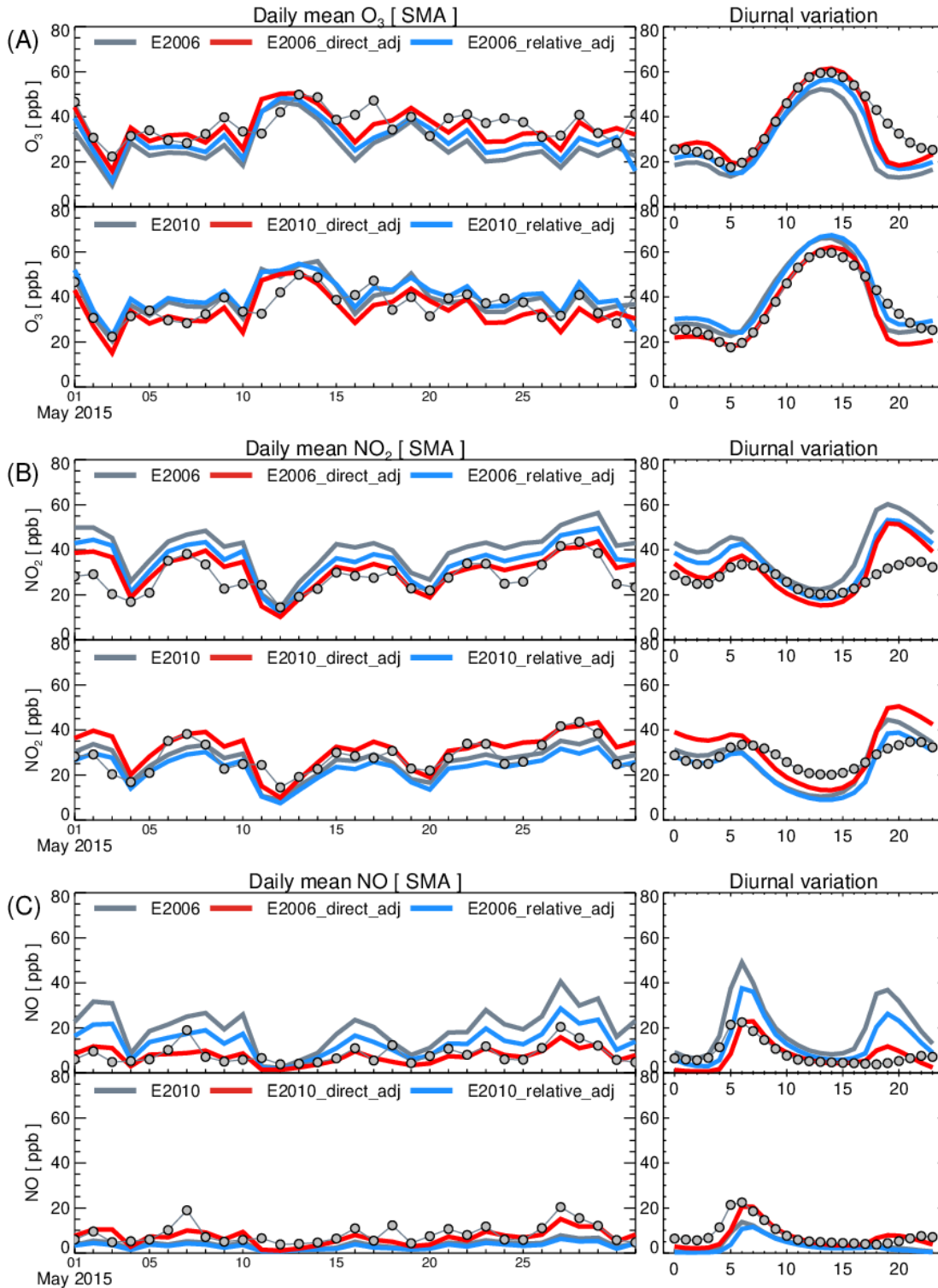
577

578



579

580 Fig. 1. Comparison of monthly total bottom-up NO_x emissions and adjusted NO_x emissions for major metropolitan
 581 areas in East Asia: (A) Beijing, (B) Shanghai, (C) SMA, and (D) Tokyo. The gray and black bars indicate the base
 582 emission inventories, i.e. E2006 and E2010 for each emission inventory, respectively.

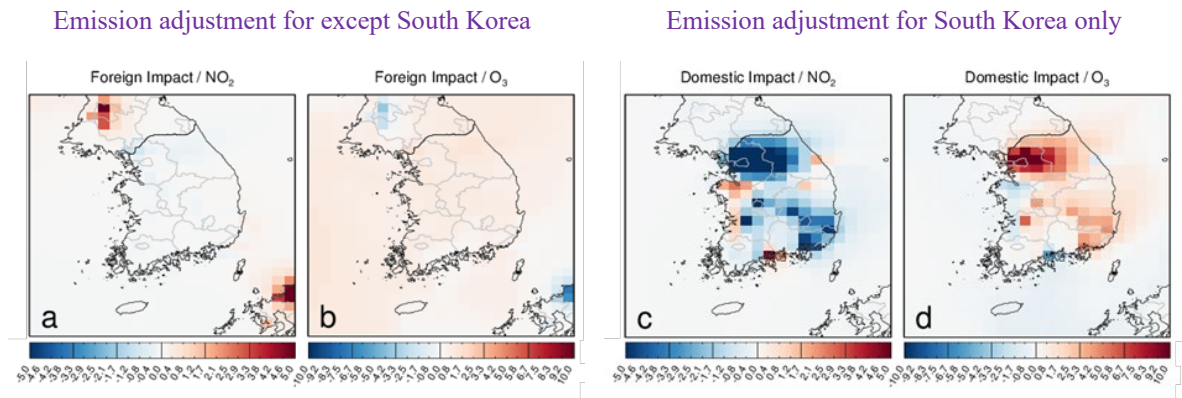


583

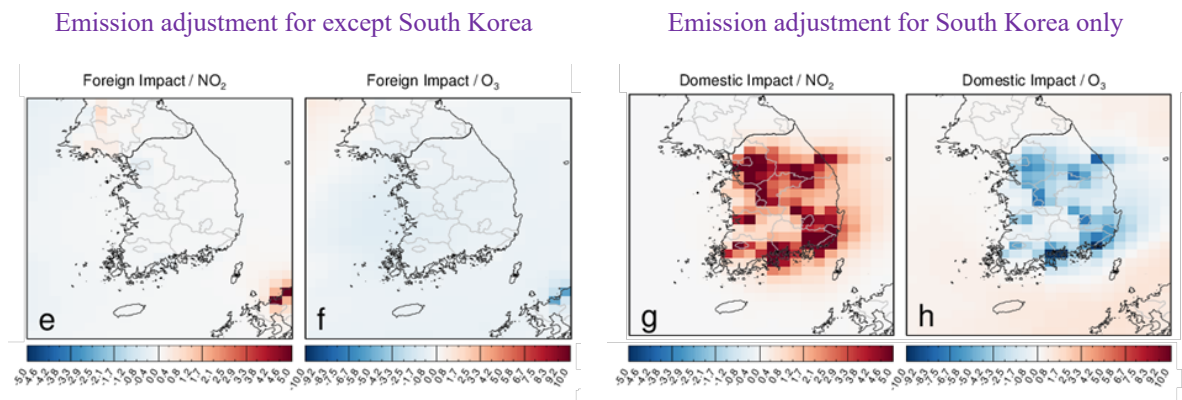
584 Fig. 2. Time series of the daily mean (left) and diurnal variation (right) of (a) O₃ concentrations, (b) NO₂
 585 concentrations, and (c) NO concentrations in the SMA. The gray lines indicate the base CMAQ simulations using
 586 the E2006(INTEX-B 2006/CAPSS 2007) (top) and E2010(MICS-Asia 2010/CAPSS 2010) (bottom) emissions
 587 inventories, respectively. The red and blue lines indicate the CMAQ simulations using the adjusted NO_x emissions
 588 based on the direct and relative adjustment methods, respectively.

589

Sensitivity run using E2006 with direct NO_x adjustment



Sensitivity run using E2010 with direct NO_x adjustment



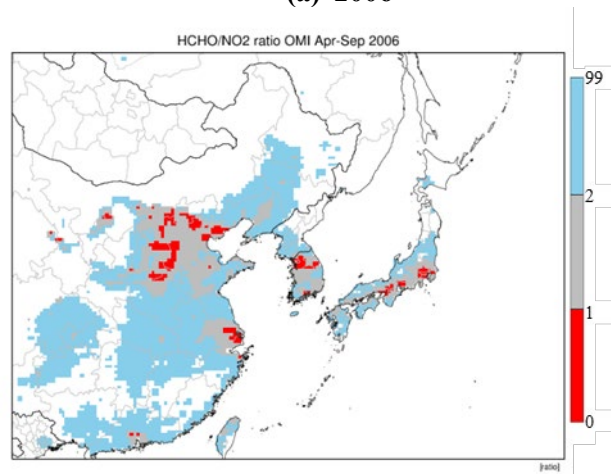
590 Fig. 3. Spatial distributions of the estimated impacts caused by the direct adjustment of foreign and domestic
591 emissions to NO₂ and O₃ concentrations in South Korea. The direct adjustment method is used on the E2006
592 (upper) and E2010 (lower) base runs.

593

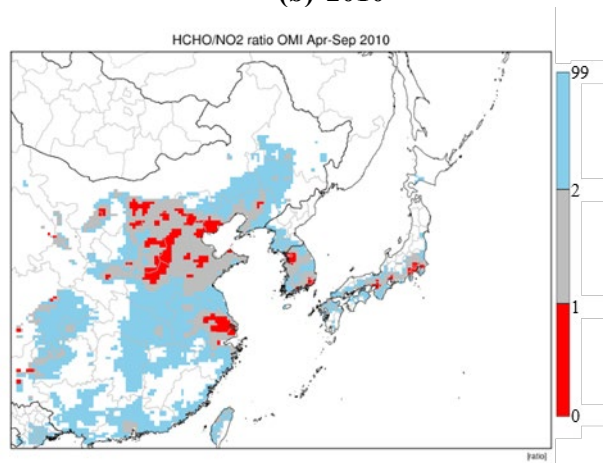
594

595

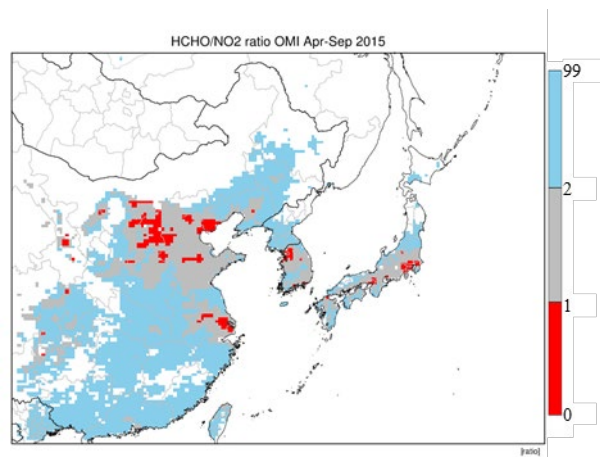
(a) 2006



(b) 2010



(c) 2015



596 Fig. 4. Spatial distributions of the OMI HCHO/NO₂ column density ratios averaged for April to September 2006,
597 2010, and 2015.

598

599